Carbohydrate Polymers 87 (2012) 2683–2689

Contents lists available at SciVerse ScienceDirect

Carbohydrate Polymers

journal homepage: www.elsevier.com/locate/carbpol

Inter-connecting pores of chitosan scaffold with basic fibroblast growth factor modulate biological activity on human mesenchymal stem cells

Min Sup Kim, Sang Jun Park, Bon Kang Gu, Chun-Ho Kim*

Laboratory of Tissue Engineering, Korea Institute of Radiological and Medical Science, Seoul 139-240, Republic of Korea

ARTICLE INFO

Article history:
Received 3 September 2011
Received in revised form
15 November 2011
Accepted 17 November 2011
Available online 26 November 2011

Keywords:
Inter-connecting micropores
Porous chitosan scaffolds
Ultrasonication
Layer-by-Layer method
Heparin binding growth factors
bFGF
Human mesenchymal stem cells

ABSTRACT

In this study, we developed bio-active molecules immobilized chitosan scaffolds with controlled pore architectures for enhanced viability of human mesenchymal stem cells (hMSCs). The decreasing in molecular weight of chitosan by ultrasonication of chitosan solution was effective in the formation of porous chitosan scaffolds, resulting in an increase of inter-connecting micropores (~10 μm) between macropores. Using a layer-by-layer method, we then prepared heparin-coated chitosan scaffolds as depots for basic fibroblast growth factors (bFGF). Enzyme-linked immunosorbent assays confirmed that heparin-coated chitosan scaffolds could bind higher amount of bFGF (24.21 ng/mg) compared to 2.53 ng/mg of non-coated scaffold. Moreover, we were able to manipulate the release profiles of bFGF from the scaffolds for 7 days. *In vitro* studies showed that chitosan scaffolds induced the improved viability and proliferation of hMSCs through their synergetic effects of the inter-connecting micropores and the sustained released of bFGF. Our results suggest that bFGF immobilized chitosan scaffolds with controlled inter-connecting pores, in combination with other heparin-binding growth factors, have potential implants for controlling biological functions in regenerative medicine.

1. Introduction

Chitosan, a partially deacetylated chitin composed of glucosamine and *N*-acetyl-D-glucosamine in a β(1–4) linkage, offers a number of advantages as a candidate scaffolding material for tissue engineering applications; notably, it is non-immunogenic, biocompatible, biodegradable, and possesses hemostatic properties (Muzzarelli et al., 2011). Moreover, previous research of chitosan scaffolds with controlled porous structures has shown that an interconnected-pore structure is favorable for the diffusion of gases and nutrients necessary to support cell growth as well as the in-growth of large numbers of cells *in vitro* and *in vivo* (Choi, Xie & Xia, 2009; Ko, Kawazoe, Tateishi & Chen, 2010).

Recent years have seen a number of efforts to accelerate tissue regeneration, including attempts to incorporate therapeutic proteins, such as growth factors and specific peptides, into porous scaffolds (Kobsa & Saltzman, 2008; Tan, Choong & Dass, 2010). Basic fibroblast growth factor (bFGF), which can stimulate proliferation of various cell types and act as a potent mitogen for tissue regeneration, wound healing and angiogenesis, is a representative therapeutic protein that has been widely used in tissue-engineering and drug-delivery applications (Tayalia & Mooney, 2009). However, bFGF rapidly denatured under physiological conditions, prompting research into the use of heparin as a means to maintain the biological activity and control the release profile of bFGF (Murphy & Mooney, 1999). Heparin, a highly sulfated glycosaminoglycan containing negatively charged carboxylic and sulfonic groups, is capable of binding to several growth factors, including bFGF as well as vascular endothelial growth factor (VEGF) and platelet derived growth factor (PDGF), with high affinity through interaction with the heparin-binding domains of these proteins (Lee, Silva & Mooney, 2010). Importantly, the interactions between heparin and heparin-binding growth factors are reversible and depend on the physiological properties of the surrounding environment. Heparin has been incorporated into scaffolds using various methods, including physical blending, biochemical conjugation, and the layer-by-layer (LBL) method (Nie, Baldwin, Yamaguchi & Kiick, 2007; Pavinatto, Caseli & Oliveira Jr., 2010).

The LBL method is advantageous in that functional substrates are created in an aqueous environment through a gentle process that preserves the activity of fragile proteins. In the LBL method, positively and negatively charged polymers are adsorbed sequentially onto a charged surface. This LBL method can be used to develop functional scaffolds composed of positively charged

* Corresponding author at: Laboratory of Tissue Engineering, Korea Institute of Radiological and Medical Sciences, 215-4, Gongneung-dong, Nowon-gu, Seoul 139-706, Republic of Korea. Tel.: +82 2 970 1319; fax: +82 2 970 1317.
E-mail address: chkim@kcch.re.kr (C.-H. Kim).

0144-8617/$ – see front matter.
doi:10.1016/j.carbpol.2011.11.060

polymeric substrates and negatively charged polymers with therapeutic proteins (Ariga, McShane, Lvov, Ji & Hill, 2011; Ma, Zhou, Gao & Shen, 2007; Muzzarelli, 2011).

Our ultimate goal is to develop novel scaffolds that provide a biomimetic environment capable of promoting or suppressing specific biological signals as natural ECM would. Here, we fabricated chitosan scaffolds with controllable pore architectures containing depots of the growth factor, bFGF. We accomplished this by exploiting decreased molecular weight chitosan solutions, created using ultrasonic treatment, and heparin coating with the LBL method. The objectives of our study were as follows: (1) to investigate the pore architectures of chitosan scaffolds as a effect of molecular weight; (2) to evaluate heparin and bFGF binding to chitosan scaffolds; (3) to monitor the *in vitro* release profile of heparin-bound bFGF; and (4) to assess the effects of pore architectures and released bFGF on the viability of human mesenchymal stem cells (hMSCs) *in vitro*.

2. Materials and methods

2.1. Materials

Chitosan powder (average MW, 370 kDa; deacetylation degree, 85%), heparin sodium salt (average MW, 15 kDa), and toluidine blue O (TB; MW, 305.83 kDa) were purchased from Sigma–Aldrich (St. Louis, MO, USA). Acetic acid (extra-pure grade) was purchased from JUNSEI Chemical Industries (Chuo-ku, Osaka, Japan). Butanol was purchased from Tokyo Chemical Industry (Kita-Ku, Tokyo, Japan). Ethanol (absolute for analysis) was purchased from Merck (Darmstadt, Germany). Paraformaldehyde, Triton X-100, dimethyl sulfoxide (DMSO), sucrose (MW, 342.24), lysozyme (from chicken egg white, 47,700 units/mg, #117K1547) and ethylene diamine tetra acetic acid (EDTA) were purchased from Sigma–Aldrich. Bovine serum albumin (BSA) Fraction V (from bovine blood) was purchased from Amersham/USB (Arlington Heights, IL, USA). bFGF (MW, 17.3 kDa) was purchased from Peprotech (Rocky Hill, NJ, USA). Low-glucose, Dulbecco's Modified Eagle's Medium (DMEM), Dulbecco's phosphate buffered saline (DPBS), and 0.05% trypsin–EDTA were purchased from Gibco BRL (Carlsbad, CA, USA). Fetal bovine serum (FBS) and penicillin–streptomycin (p/s) were purchased from Wel Gene Inc. (Daegu, South Korea). Cell Counting Kit-8 (CCK-8) was purchased from Dojindo Laboratories (Kumamoto, Japan).

2.2. Preparation of chitosan scaffolds with controlled molecular weights

First, chitosan powder was purified to remove impurities; then 1% chitosan powder (wt/v) was dissolved in 1% acetic acid (v/v) at 4 °C until the solution became transparent, and homogeneous. The resulting chitosan solution was filtered through glass filters (25G2) to remove impurities. The filtrate was precipitated by adding 1 M NaOH, and washed by deionized (DI) water until neutral pH. Then, the resulting chitosan was lyophilized for 2 days. Chitosan scaffolds were fabricated as described in our previous studies (Lim et al., 2007). Briefly, chitosan solutions, prepared by dissolving 2% purified chitosan (wt/v) in 1% acetic acid (v/v), were ultrasonicated at 4 °C for 0, 30, 60, 90, and 120 min using an ultrasonicator (HD2070, BANDELIN, Berlin, Germany) to achieve different molecular-weight solutions. Then, ultrasonicated 2% (wt/v) chitosan solutions were diluted to 1% chitosan by adding 16% (v/v) butanol (dissolved in 1% acetic acid) and stirring for 1 h. The resulting chitosan solutions were lyophilized for 1 day, and then washed sequentially with 100%, 70% and 50% ethanol, and DI water for 1 h each. After washing, the morphology of finished scaffolds, designated CS 0, CS 30, CS 60, CS 90, and CS 120 corresponding to ultrasonication times of 0, 30, 60, 90, and 120 min, respectively, was characterized by a MIRA II field emission-scanning electron microscope (FE-SEM; Tescan, Libusinatr, Czech Republic).

2.3. Viscosity of chitosan solutions

We investigate the decreased viscosity of ultrasonicated solution with AR 2000 EX rheometer (TA instrument, New Castle, DE, USA) using a cone and plate geometry of 4 cm diameter and 1° cone angle. 1% (wt/v) of each chitosan scaffolds dissolved in 1% (v/v) acetic acid solution and chitosan solution subjected into rotational cone and plate at controlled shear rates. The viscosity of chitosan solutions was measured at 20 °C for 5 min with a constant shear stress of 1 Pa.

2.4. Fourier transform-infrared analysis

The chemical integrity of chitosan scaffolds was investigated by Fourier transform-infrared (FTIR) spectroscopy (Tensor 27; Bruker Optics, Ettlingen, Germany). The scaffold was cut into small pieces for the preparation of KBr discs and FTIR spectra over a range from 4000 to 500 cm^{-1} was recorded.

2.5. Degradation of chitosan scaffolds in vitro

The degradation behavior of chitosan scaffolds was determined *in vitro* by measuring changes in the weight of samples treated with lysozyme over time under specific conditions. The initial dry weight of each scaffold was determined and recorded as W1. The scaffolds were sterilized in 70% ethanol for 30 min under a UV lamp and washed sequentially in DPBS for 30 min. After sterilization, 10 mg of scaffolds were incubated in 1 ml of lysozyme solution (50 μg/ml in DPBS) under standard cell culture conditions (37 °C, 5% CO_2) for up to 4 weeks. Lysozyme solutions were replaced weekly with freshly prepared solutions. Scaffolds were collected after 1, 2, 3, and 4 weeks, washed with DI water, and lyophilized. The remained weight of the lyophilized scaffolds was recorded as W2, and calculated as a percentage of the starting weight using following equation: The percentage of remained weight (%) = 100 × (W2/W1).

2.6. Fabrication of bio-active molecules immobilized chitosan scaffolds

Heparin-coated chitosan scaffolds were fabricated using the LBL method. Chitosan scaffolds and heparin were prepared as positively and negative charged polymers, respectively. First, each scaffold (CS 0, 30, 60, 90, and 120) was immersed in a 2 mg/ml heparin solution (dissolved in DPBS) at room temperature for 30 min. After washing heparin-coated scaffolds (CS-H 0, 30, 60, 90, and 120) three times for 30 min with DPBS, a bFGF solution (100 ng/ml bFGF, 0.1% BSA, 5% sucrose, and 0.01% EDTA) was added and allowed to react with CS-H scaffolds for 30 min. The resulting heparin and bFGF immobilized scaffolds (CS-HB 0, 30, 60, 90, and 120) were washed three times for 30 min with DPBS. Chitosan scaffolds containing passively adsorbed bFGF (CS-PA 0, 30, 60, 90, and 120) were prepared as controls.

2.7. Investigation of heparin on chitosan scaffolds

Negatively charged ionic groups of heparin on chitosan scaffolds were quantified using TB staining assays, as previously described (Kim et al., 2010). Briefly, scaffolds were immersed in a 0.1 mM TB solution for 1 h at room temperature, and the ionic complexes of TB on the scaffolds were dissolved by reacting with a mixture of 0.1 M NaOH and ethanol (1:4, v/v). The optical density (OD) of each sample was then measured at 640 nm using a plate reader (Spectra Max M2e; Molecular Devices, Sunnyvale, CA, USA).

Heparin on the chitosan scaffold (CS 60) was observed by immobilizing 0.1 mM fluorescein isothiocyanate (FITC)-labeled heparin (Invitrogen, Carlsbad, CA, USA) on the scaffold, as previously described above. Scaffolds containing FITC-labeled heparin were visualized using confocal laser scanning microscopy (CLSM, C1; Nikon Corp., Chiyoda-ku, Japan).

2.8. Analysis of heparin-bound bFGF on chitosan scaffolds

bFGF bound to heparin on chitosan scaffolds was quantified by measuring the amount of bFGF remaining in solution after incubating with CS-H scaffolds using an enzyme-linked immunosorbent assay (ELISA) kit (Invitrogen). A standard calibration curve was prepared using solutions containing known concentrations of bFGF.

The release kinetics of bFGF from chitosan scaffolds was determined by incubating samples in 5 ml of PBS at 37 °C for up to 7 days with continuous agitation. Samples (100 μl) were collected at designated time points. The cumulative amount of released bFGF was determined using the same ELISA kit, as described above.

2.9. Viability of hMSCs on chitosan scaffolds

Two *in vitro* tests were conducted to evaluate the viability of hMSCs (Lonza, Basel, Switzerland) on chitosan scaffolds. During the first test, the viability of hMSCs on scaffolds with different pore structures was investigated. In the second test, the synergetic effects of inter-connecting pore structure and released bFGF were evaluated using hMSCs cultured on chitosan scaffolds. Before *in vitro* tests, CS 0, CS 60, and CS 120 were prepared for analysis of the effect of pore structure, and CS 0 (control), CS-PA 0, CS-HB 0, and CS-HB 60 were prepared for evaluation of the effects of released bFGF. All scaffolds were prepared as circular shapes (diameter: 15 mm). hMSCs were maintained in DMEM supplemented with 10% FBS and 1% p/s under standard culture conditions (37 °C, 5% CO_2). When the cells had reached approximately 70% confluence, they were enzymatically detached using trypsin/EDTA and seeded onto the scaffolds at a density of 2×10^3 cells/cm^2 (passage 7) in DMEM with 10% FBS and 1% p/s. For evaluating the effects of pore structure, fresh medium with the same composition (DMEM with 10% FBS and 1% p/s) was added after 1 day in culture. For evaluating the effects of bFGF released from scaffolds, the medium was changed to DMEM containing 1% FBS and 1% p/s. The viability of hMSCs grown on scaffolds was evaluated at designated time points using CCK-8 assays.

2.10. Immunofluorescence staining of hMSCs cultured on chitosan scaffolds

At 1 and 7 days post-seeding, hMSCs cultured on CS 0 (control), CS-PA 0, CS-HB 0 and CS-HB 60 were immune stained using Alexa Fluor 488 phalloidin (Invitrogen) and propidium iodide (Sigma Aldrich) for actin filaments and nuclei, respectively. Cells on scaffolds were investigated using CLSM; fluorescence images were obtained from a depth of 150 μm.

2.11. Statistical analysis

Quantitative data were obtained in triplicate and are reported as means ± standard deviations, where indicated. Statistical analyses were performed using a one-way analysis of variation (ANOVA), followed by Tukey HSD for multiple comparisons. A p-value < 0.05 was considered statistically significant.

3. Results and discussion

In order to the controlled molecular weight of chitosan, chitosan solutions were ultrasonicated for 0, 30, 60, 90, and 120 min. And then, we investigated the viscosity of chitosan solutions as an effect of ultrasonication time (data was not shown). The viscosity of CS 0 solutions was 299.63 ± 0.21 mPa·s; the viscosity of scaffold solutions decreased with increasing ultrasonication time to 230.44 ± 0.32 mPa·s (CS 30), 195.40 ± 0.15 mPa·s (CS 60), 155.04 ± 0.11 mPa·s (CS 90), and 126.46 ± 0.17 mPa·s (CS 120). From FTIR spectrum of chitosan scaffolds, we observed a broad hydroxyl band near 3400 cm^{-1} in all samples attributable to the –OH stretching mode (data was not shown). Characteristic peaks at 2932, 1675, 1411, 1385, and 1240 cm^{-1} due to CH_2 stretching, amide I, OH vibration, CH_3 bending, and amide III, respectively, were also observed in all samples. FTIR spectral analyses showed that the changes caused by ultrasonication treatment did not involve effects on the chemical integrity of chitosan scaffolds, but instead reflected partial breaks of β-linkage in chitosan (Wu, Zivanovic, Hayes & Weiss, 2008). These results indicate that ultrasonication was an effective method for controlling the molecular weight of chitosan.

In previous studies, we confirmed that addition of butanol, and the resulting phase separation between the chitosan solution and butanol, produces chitosan scaffolds with a well defined porous structure, characterized by inter-connecting smaller micropores (size, ~10–60 μm) between larger micropores. Moreover, the proportion of smaller micropores increased with increasing concentrations of butanol (Lim et al., 2007). On the basis of these previous studies, we investigated the morphological changes in chitosan scaffolds (prepared using a constant, lower concentration of butanol) due to ultrasonication of chitosan solutions. As shown in Fig. 1, lyophilized chitosan scaffolds exhibited porous structures. However, a porous structure with small micropores (~10 μm) in the frame of chitosan scaffolds with large micropores (80–100 μm) was observed only in CS 60, 90, and 120; the others contained only larger pores. In a previous study, chitosan solutions with lower molecular weights yielded lyophilized chitosan scaffolds with smaller pores (Chung et al., 2002). In the present study, we found that chitosan solutions with lower molecular weights, which have higher diffusion rates due to lower viscosity, exhibited enhanced formation of smaller and inter-connecting micropores (~10 μm) through thermally induced phase separation between chitosan solutions and butanol during lyophilized process of chitosan scaffolds. These results indicate that the molecular weights of chitosan solutions determine the size and inter-connectivity of pores in chitosan scaffolds.

We next investigated lysozyme-mediated degradation of chitosan scaffolds as an effect of molecular weight. As shown in Fig. 2, the degradation behavior of all scaffolds in the presence of lysozyme followed a similar trend. For examples, the initial weight remaining of CS 0, 30, 60, 90, and 120 were 95.4 ± 1.63, 95.5 ± 1.29, 94.25 ± 0.96, 94.51 ± 1.27, and 95.25 ± 1.71%, respectively, at 2 weeks; the corresponding values at 4 weeks were 86.5 ± 5.26, 89.25 ± 2.75, 87.25 ± 2.98, 85.75 ± 2.56, and 88.25 ± 2.63%, respectively. Ren et al. reported that the enzymatic degradation of chitosan depended on its degree of deacetylation (DD); chitosan with a lower DD was degraded faster by lysozyme than chitosan with a higher DD (Ren, Yi, Wang & Ma, 2005). Using a previously described method, we calculated DD values for our chitosan scaffolds from hydroxyl and amide I bands of FTIR analysis (Baxter, Dillon, Anthony Taylor & Roberts, 1992). The calculated DD values were 82.03%, 82.43%, 82.44%, 82.37%, and 82.94% for CS 0, 30, 60, 90, and 120, respectively. The similarity of the DD values of chitosan scaffolds regardless of its molecular weights is consistent with the molecular weight-independent degradation behaviors shown in Fig. 2. In agreement with this, previous research showed that there

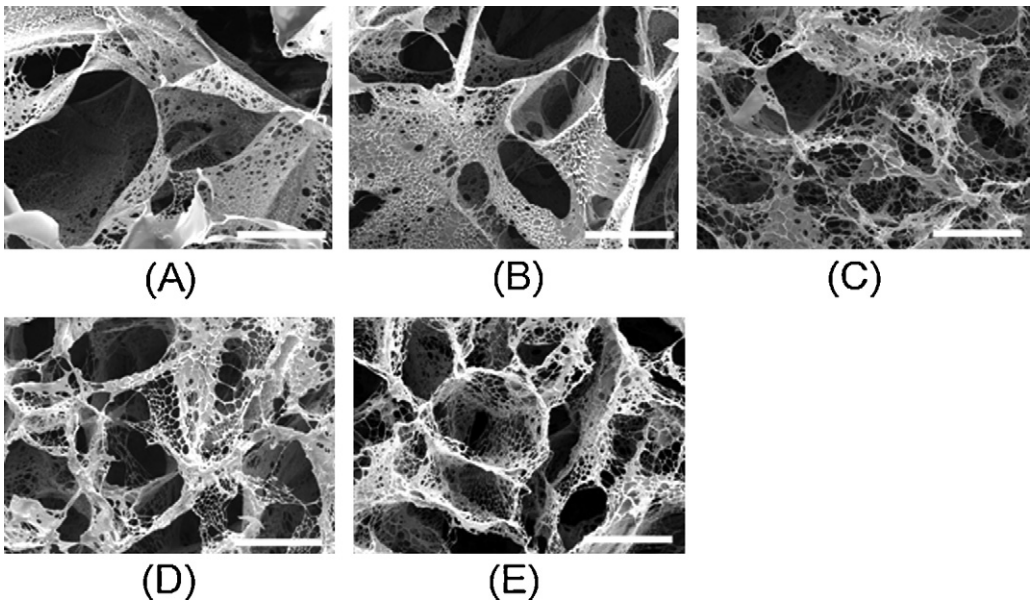

Fig. 1. Representative SEM images of chitosan scaffolds: (A) CS 0, (B) CS 30, (C) CS 60, (D) CS 90, and (E) CS 120, prepared using ultrasonication of 0, 30, 60, 90, and 120 min, respectively. Smaller and inter-connecting micropores (~10 μm) were observed on CS 60, 90, and 120. Scale bar is 100 μm.

was no relationship between ultrasonication treatment and DD values of chitosan (Fan, Saito & Isogai, 2008; Wu, Zivanovic, Hayes & Weiss, 2008).

We quantified the amount of coated heparin on porous chitosan scaffolds using TB assay for immobilization of bio-active molecules. As shown in Fig. 3A, the amount of TB taken up by CS 0 (without heparin) was 0.06 ± 0.02 mM, a value that increased to 0.30 ± 0.04 and 0.32 ± 0.05 mM for CS-H 0 and CS-H 30, respectively, after the reaction with heparin. In the case of chitosan scaffolds with inter-connecting micropores, the amount of TB taken up by CS-H 60 increased to 0.44 ± 0.09 mM, which represented the saturation point; chitosan scaffolds beyond CS-H 60 exhibited slight increase in TB uptake upon reacting with heparin. Photographs of TB-stained scaffolds illustrate this trend in TB uptake (Fig. 3B). To visualize heparin on chitosan scaffolds (CS 60), we coated FITC-heparin on scaffolds. The resulting fluorescence images confirmed that coated heparin was not affected by the thickness of scaffolds. Heparin could be observed throughout cross-sectional areas of samples, reflecting the inter-connecting pore structure of scaffolds, as shown in Fig. 4. These results suggest that the increased surface area of chitosan scaffolds caused by inter-connecting micropores increased the amount of coated heparin and confirm that the controlled molecular weight of chitosan and LBL method were effective for heparin coating on scaffolds.

Next, the amount of immobilized bFGF on chitosan scaffolds was evaluated using ELISA. As shown in Fig. 5A, the amount of passively

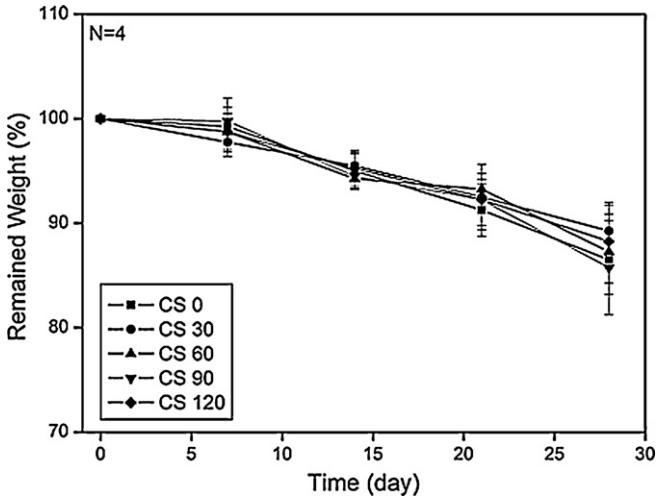

Fig. 2. Enzymatic degradation of chitosan scaffolds incubated at 37 °C for up to 4 weeks in a 50 μg/ml lysozyme solution.

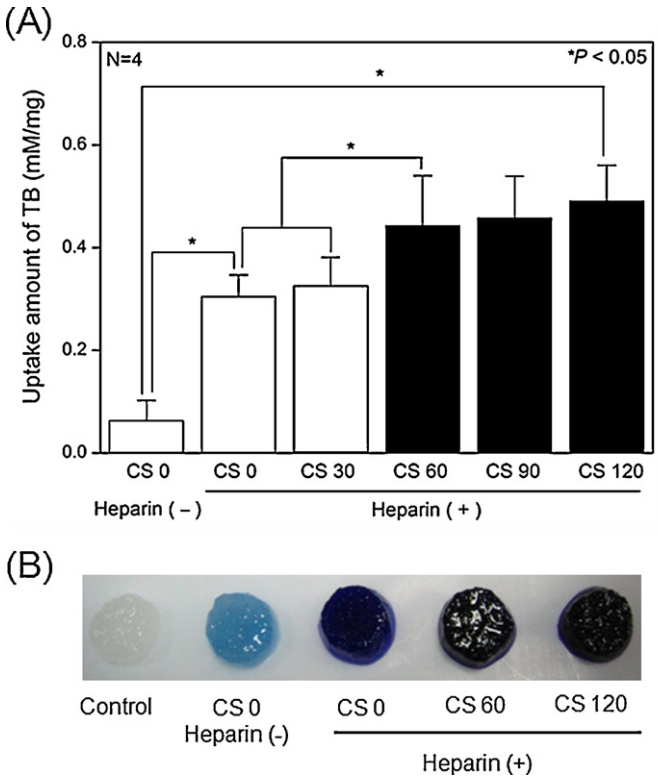

Fig. 3. (A) Quantification of negatively charged functional heparin groups on chitosan scaffolds, analyzed by TB-uptake assays. The number of negatively charged groups on chitosan scaffolds significantly increased after heparin coating. (B) Photograph of TB-stained chitosan scaffolds.

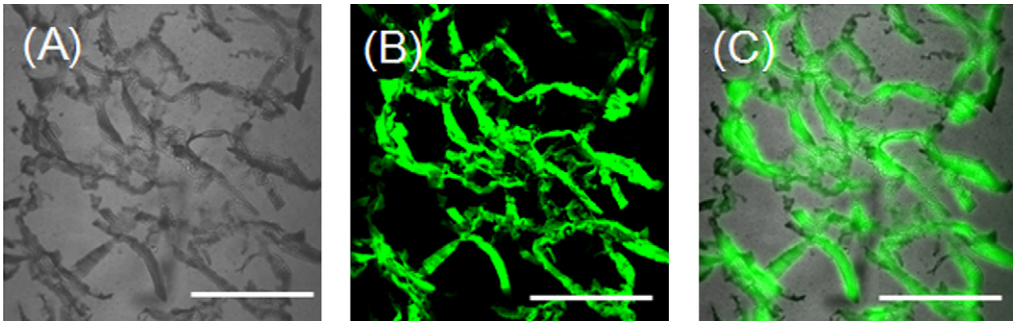

Fig. 4. Fluorescence images of FITC-heparin on chitosan scaffolds: (A) phase-contrast, (B) fluorescence, and (C) merged images. FITC-heparin was observed throughout the cross-sectional areas of scaffolds. Scale bar is 500 μm.

absorbed bFGF on CS-PA 0 was 2.53 ± 0.28 ng/mg. Notably, the presence of heparin and inter-connecting micropores substantially increased bFGF binding to chitosan scaffolds; in groups of CS-HB 0, CS-HB 60, and CS–HB 120, the amount of bound bFGF was 12.10 ± 1.97, 20.77 ± 2.31, and 24.21 ± 3.01 ng/mg, respectively. These trends were consistent with the quantification results of heparin (Fig. 3A). Heparin is able to bind to several growth factors with high affinity and specificity (Lee, Silva & Mooney, 2010). In the case of bFGF, these interactions are primarily due to electrostatic binding between positively charged amino groups of the arginine- and lysine-rich bFGF molecule and negatively charged sulfonyl and carboxyl groups in heparin (Tayalia & Mooney, 2009; Uebersax, Merkle & Meinel, 2009).

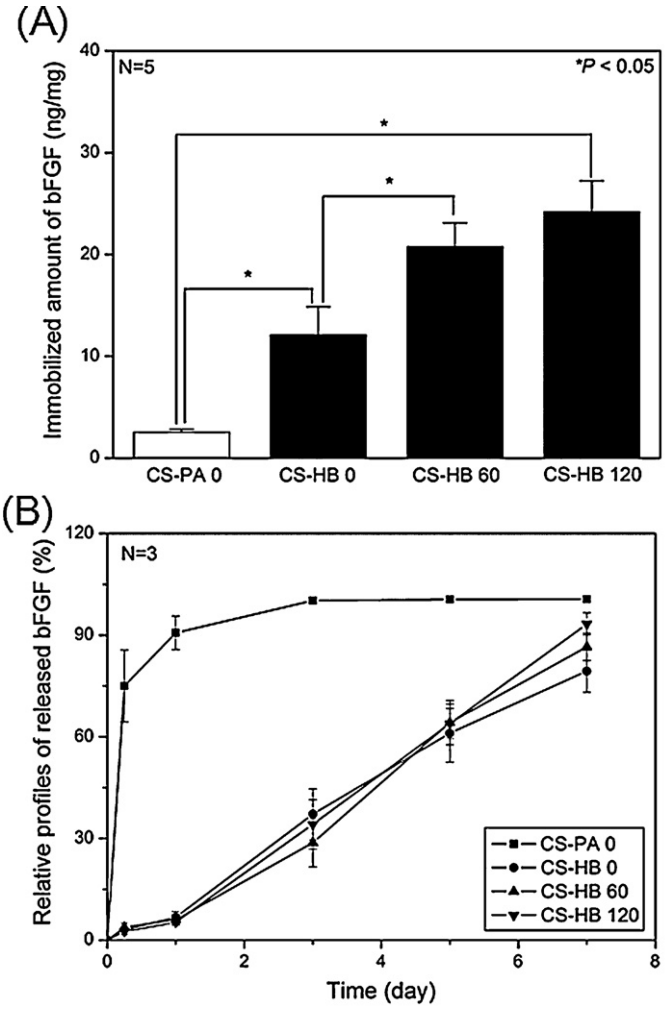

Fig. 5. (A) Quantification of bFGF on chitosan scaffolds by ELISA. The amount of immobilized bFGF on scaffolds was greater than that in groups without heparin. (B) Release profiles of bFGF from scaffolds incubated in PBS at 37 °C (CS-PA and CS-HB were abbreviated by passively bFGF absorbed on chitosan scaffolds and bFGF immobilized on heparin coated chitosan scaffolds, respectively).

The release profiles of bFGF from chitosan scaffolds are shown in Fig. 5B. Scaffolds containing passively adsorbed bFGF (CS-PA 0) showed an initial burst of bFGF release, amounting to 74.99 ± 10.61% and 90.72 ± 4.91% of initial bFGF on days 1 and 3, respectively; thereafter, no further release of bFGF was observed. However, bFGF immobilized scaffolds (CS-HB 0, 60, and 120) was released over the course of 7 days. For example, immobilized bFGF on CS-HB 0, 60, and 120 was released at rates of 6.72 ± 1.73%, 6.06 ± 1.45% and 5.33 ± 0.89%, respectively, at day 1; the corresponding values at day 7 were 79.36 ± 6.21%, 86.56 ± 4.07%, and 93.29 ± 3.26%, respectively. The release of bFGF from heparin-coated scaffolds appeared to be linear with minimal burst release, regardless of the amount of immobilized bFGF on the scaffolds. Our results indicate that heparin-coated chitosan scaffolds control the release of bFGF, and also strongly protect bFGF from degradation.

In aspect of scaffolds for tissue formation, the pore architectures are known to play a critical role in tissue engineering, as it provides the vital framework for the seeded cells to organize into a functional tissue (Hollister, 2005). The pore architectures of scaffolds have been presented in previous studies, which showed that pore size and inter-connectivity of scaffolds are critical factors in the regulation of hMSCs proliferation and differentiation (Hu, Feng, Liu & Ma, 2009; Kasten et al., 2008; Majd et al., 2009; Ragetly et al., 2010). In this study, we controlled the pore size (pore sizes ranging from 10 to 100 μm) of chitosan scaffolds by not only different molecular weight of chitosan, but also addition of non-solvent to chitosan solution. To evaluate the effects of the pore architectures of chitosan scaffolds on cellular attachment and proliferation, hMSCs were seeded on scaffolds.

Fig. 6A shows the viability of hMSCs on chitosan scaffolds with different pore architectures. On day 1, the viability of hMSCs was similar, exhibiting OD values on CS 0, 60, and 120 of 0.42 ± 0.06, 0.46 ± 0.04, and 0.45 ± 0.05, respectively, in CCK-8 assays. However, on day 4, the OD values of CS 60 and 120 increased significantly to 0.79 ± 0.04 and 0.75 ± 0.04, respectively, whereas that of the CS 0 increased only slightly (0.59 ± 0.04). By comparison, conventional chitosan scaffolds with only large micropores (CS 0) showed limited regulation of cellular behavior (Fig. 6A). However, our results suggest that CS 60 and 120 with the controlled pore size and inter-connectivity (SEM images in Fig. 1) were able to actively supply gas and nutrients to cultured hMSCs on scaffold. Indeed, fluid and gas flow through the scaffolds is a combination of various important factors: porosity, size, distribution of pore, and their

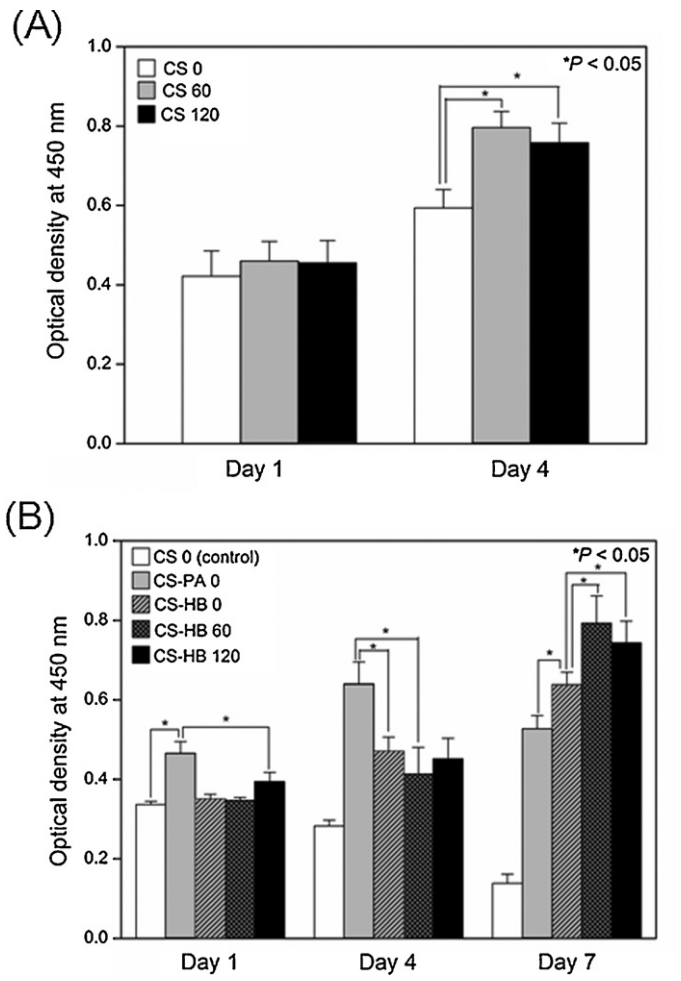

Fig. 6. The viability of hMSCs on chitosan scaffolds. (A) hMSCs cultured on CS 0, 60, and 120 in conventional media for 4 days. (B) hMSCs cultured on CS 0 (control), CS-PA 0, CS-HB 0, CS-HB 60, and CS-HB 120 in conditioned media for 7 days.

inter-connectivity (Lee, Cuddihy & Kotov, 2008). During our *in vitro* study, differences in those pore architectures could therefore affect hMSCs and nutrient interaction, possibly resulting in better proliferation for one scaffold type compared to the other. In our previous study, we also found similar results using human dermal fibroblasts on chitosan scaffolds containing inter-connecting micropores (created by preparing with different butanol content) (Chun, Kim & Kim, 2008). Consistent with these results, Kasten et al. reported that scaffolds with smaller and inter-connecting pore size (<40 μm) induced higher proliferation and the ECM protein content of hMSCs, since facilitated transport of oxygen and nutrients to hMSCs, compare to the scaffolds with bigger pore size (<136 μm) (Kasten et al., 2008).

bFGF is generally implicated in the enhancement of *in vitro* formation of focal adhesion and proliferation of various types of cell in a concentration-dependent manner. To assess the biological activity of bFGF released from the chitosan scaffolds, we first tested the effect of soluble bFGF on the proliferation of hMSCs according to the previous study, and found that greater than 5 ng/ml bFGF was effective concentration (Schmidt et al., 2006). As shown in Fig. 6B, on day 1, the viability of hMSCs treated with conditioned media obtained after incubating scaffold containing passively adsorbed bFGF (CS-PA 0) was higher (OD = 0.47 ± 0.03) than that of CS-HB 0 (0.33 ± 0.02), CS-HB 60 (0.35 ± 0.01), CS-HB 120 (0.34 ± 0.02), and CS-0 (control; 0.39 ± 0.02). This trend extended to day 4, when the OD values of the CS-PA 0 increased to 0.64 ± 0.05. However, the trend was reversed on day 7, at which point the proliferation of cultured hMSCs in CS 0 and CS-PA 0 significantly decreased compared to the other groups. These results may reflect the burst-type pattern of bFGF release from CS-PA 0, in which approximately 95% of bFGF was released within 3 days (Fig. 5B). However, the sustained release of bFGF from the heparin-coated CS-HB 0, 60, and 120, which might maintain effective concentration of bFGF in culture medium, resulted in the continuous proliferation of hMSCs. Similar results have been reported that bFGF released from a heparin-incorporated system enhanced the proliferation of hMSCs *in vitro* to a greater extent than bFGF released from passively adsorbed groups (Ariga, McShane, Lvov, Ji & Hill, 2011; Benoit, Collins & Anseth, 2007). The proliferation of hMSCs on CS-HB 60 and 120, in particular, was significantly increased compared to that on CS-HB 0. These trends correlated with the results of Fig. 6A: inter-connecting micropores on CS-HB 60 and 120 accelerated the viability of hMSCs regardless of the amount of bFGF bound to chitosan scaffolds (CS-HB 0, 60, and 120). Our *in vitro* studies showed that the viability and proliferation of hMSCs was enhanced through the synergetic effects of inter-connectivity between macropores and the sustained released of bFGF from chitosan scaffolds.

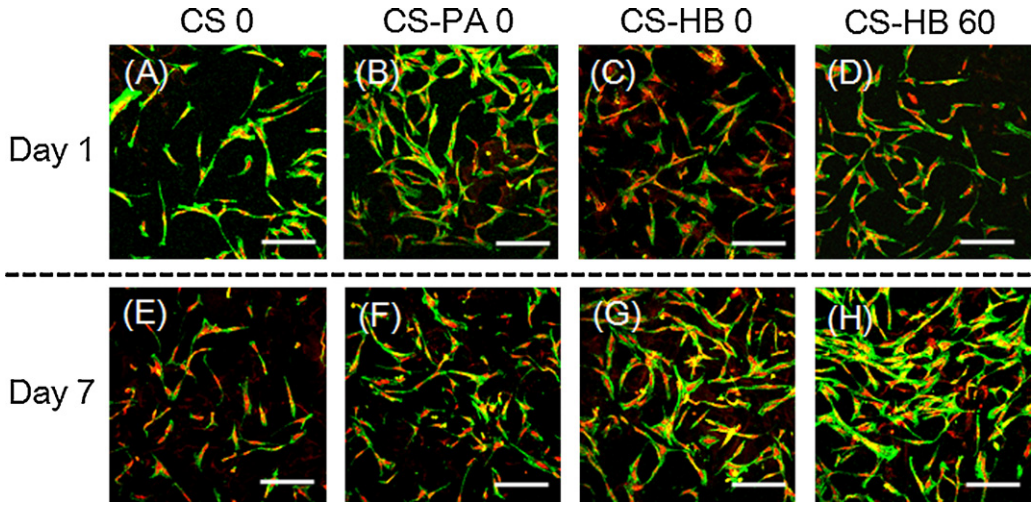

Fig. 7. CLSM images of hMSCs on chitosan scaffolds after 7 days of cultivation. Scale bar is 100 μm. Images of hMSCs on (A) CS 0 (control), (B) CS-PA 0, (C) CS-HB 0, and (D) CS-HB 60 on day 1. Images of hMSCs on (E) CS 0 (control), (F) CS-PA 0, (G) CS-HB 0, and (H) CS-HB 60 on day 7. Cell nuclei (red) and actin filaments (green) of hMSCs were stained with propidium iodide and Alexa Fluor 488 phalloidin, respectively. CLSM images were taken from 150 μm in depth. (For interpretation of the references to color in this figure legend, the reader is referred to the web version of the article.)

Finally, we confirmed the synergetic effects of pore architectures and released bFGF on hMSCs cultured on chitosan scaffolds using immunofluorescence staining. As shown in Fig. 7B, on day 1, hMSCs cultured on CS-PA 0 reached a much higher density of nuclei compared to other groups. Moreover, they were well spread out with mature formation of actin filaments. On day 7, hMSCs in CS 0 (Fig. 7E) and CS-PA 0 (Fig. 7F) exhibited a thinner spindle morphology compared to hMSCs cultured on CS-HB 0 and 60. Also, hMSCs on CS-HB 60 showed a well-spread morphology compared to those on CS-HB 0. These cellular morphologies correlate with cellular viability (Fig. 6), measured by CCK-8 assays.

4. Conclusions

In this study, we were able to manipulate chitosan scaffolds with inter-connecting micropores and amount of immobilized bFGF on scaffolds. In particular, an *in vitro* study using hMSCs revealed that the well defined architectures and presence of bFGF indicated significantly enhanced biocompatibility of chitosan scaffolds compared to ordinary chitosan scaffold. Furthermore, our chitosan system with other heparin-binding growth factors has wide-ranging application to actively control the proliferation and differentiation of various cells for tissue regeneration.

Acknowledgements

This work was supported by Industrial Strategic Technology Development Program (10035291, Multi-functional medical fiber complex technology) funded by the Ministry of Knowledge Economy (MKE, Korea) and by Nuclear Research Development Program of the Korea Science and Engineering Foundation (KOSEF) grant funded by Ministry of Education, Science and Technology (MEST, Korea) (grant codes: 2011-0002361 and 2011-0020757).

References

Ariga, K., McShane, M., Lvov, Y. M., Ji, Q., & Hill, J. P. (2011). Layer-by-layer assembly for drug delivery and related applications. *Expert Opinion on Drug Delivery*, *8*(5), 633–644.

Baxter, A., Dillon, M., Anthony Taylor, K., & Roberts, G. A. F. (1992). Improved method for IR determination of the degree of N-acetylation of chitosan. *International Journal of Biological Macromolecules*, *14*(3), 166–169.

Benoit, D. S. W., Collins, S. D., & Anseth, K. S. (2007). Multifunctional hydrogels that promote osteogenic human mesenchymal stem cell differentiation through stimulation and sequestering of bone morphogenic protein 2. *Advanced Functional Materials*, *17*(13), 2085–2093.

Choi, S. W., Xie, J., & Xia, Y. (2009). Chitosan based inverse opals: Three dimensional scaffolds with uniform pore structures for cell culture. *Advanced Materials*, *21*(29), 2997–3001.

Chun, H. J., Kim, G. W., & Kim, C. H. (2008). Fabrication of porous chitosan scaffold in order to improve biocompatibility. *Journal of Physics and Chemistry of Solids*, *69*(5–6), 1573–1576.

Chung, T. W., Yang, J., Akaike, T., Cho, K. Y., Nah, J. W., Kim, S. I., et al. (2002). Preparation of alginate/galactosylated chitosan scaffold for hepatocyte attachment. *Biomaterials*, *23*(14), 2827–2834.

Fan, Y., Saito, T., & Isogai, A. (2008). Preparation of chitin nanofibers from squid pen beta-chitin by simple mechanical treatment under acid conditions. *Biomacromolecules*, *9*(7), 1919–1923.

Hollister, S. J. (2005). Porous scaffold design for tissue engineering. *Nature Materials*, *4*(7), 518–524.

Hu, J., Feng, K., Liu, X., & Ma, P. X. (2009). Chondrogenic and osteogenic differentiations of human bone marrow-derived mesenchymal stem cells on a nanofibrous scaffold with designed pore network. *Biomaterials*, *30*(28), 5061–5067.

Kasten, P., Beyen, I., Niemeyer, P., Luginbuhl, R., Bohner, M., & Richter, W. (2008). Porosity and pore size of [beta]-tricalcium phosphate scaffold can influence protein production and osteogenic differentiation of human mesenchymal stem cells: An *in vitro* and *in vivo* study. *Acta Biomaterialia*, *4*(6), 1904–1915.

Kim, M. S., Bhang, S. H., Yang, H. S., Rim, N. G., Jun, I., Kim, S. I., et al. (2010). Development of functional fibrous matrices for the controlled release of basic fibroblast growth factor to improve therapeutic angiogenesis. *Tissue Engineering Part A*, *16*(10), 2999–3010.

Ko, Y. G., Kawazoe, N., Tateishi, T., & Chen, G. (2010). Preparation of chitosan scaffolds with a hierarchical porous structure. *Journal of Biomedical Materials Research Part B: Applied Biomaterials*, *93*(2), 341–350.

Kobsa, S., & Saltzman, W. M. (2008). Bioengineering approaches to controlled protein delivery. *Pediatric Research*, *63*(5), 513–519.

Lee, J., Cuddihy, M. J., & Kotov, N. A. (2008). Three-dimensional cell culture matrices: State of the art. *Tissue Engineering Part B Review*, *14*(1), 61–86.

Lee, K., Silva, E. A., & Mooney, D. J. (2010). Growth factor delivery-based tissue engineering: General approaches and a review of recent developments. *Journal of the Royal Society, Interface*, *8*(55), 153–170.

Lim, J. I., Kim, G. W., Na, J. S., Noh, I. S., Son, Y. S., & Kim, C. H. (2007). A novel method for porous chitosan scaffold. *Key Engineering Materials*, *342*, 65–68.

Ma, L., Zhou, J., Gao, C., & Shen, J. (2007). Incorporation of basic fibroblast growth factor by a layer-by-layer assembly technique to produce bioactive substrates. *Journal of Biomedical Materials Research Part B: Applied Biomaterials*, *83*(1), 285–292.

Majd, H., Wipff, P. J., Buscemi, L., Bueno, M., Vonwil, D., Quinn, T. M., et al. (2009). A novel method of dynamic culture surface expansion improves mesenchymal stem cell proliferation and phenotype. *Stem Cells*, *27*(1), 200–209.

Murphy, W. L., & Mooney, D. J. (1999). Controlled delivery of inductive proteins, plasmid DNA and cells from tissue engineering matrices. *Journal of Periodontal Research*, *34*(7), 413–419.

Muzzarelli, R. (2011). New techniques for optimization of surface area and porosity in nanochitins and nanochitosans. *Advances in Polymer Science: Chitosan for Biomaterials II*, *244*, 167–186.

Muzzarelli, R. A. A., Boudrant, J., Meyer, D., Manno, N., DeMarchis, M., & Paoletti, M. G. (2011). Current views on fungal chitin/chitosan, human chitinases, food preservation, glucans, pectins and inulin: A tribute to Henri Braconnot, precursor of the carbohydrate polymers science, on the chitin bicentennial. *Carbohydrate Polymers*.

Nie, T., Baldwin, A., Yamaguchi, N., & Kiick, K. L. (2007). Production of heparin-functionalized hydrogels for the development of responsive and controlled growth factor delivery systems. *Journal of Control Release*, *122*(3), 287–296.

Pavinatto, F. J., Caseli, L., & Oliveira, O. N., Jr. (2010). Chitosan in nanostructured thin films. *Biomacromolecules*, *11*(8), 1897–1908.

Ragetly, G. R., Griffon, D. J., Lee, H. B., Fredericks, L. P., Gordon-Evans, W., & Chung, Y. S. (2010). Effect of chitosan scaffold microstructure on mesenchymal stem cell chondrogenesis. *Acta Biomaterialia*, *6*(4), 1430–1436.

Ren, D., Yi, H., Wang, W., & Ma, X. (2005). The enzymatic degradation and swelling properties of chitosan matrices with different degrees of N-acetylation. *Carbohydrate Research*, *340*(15), 2403–2410.

Schmidt, A., Ladage, D., Schinkothe, T., Klausmann, U., Ulrichs, C., Klinz, F. J., et al. (2006). Basic fibroblast growth factor controls migration in human mesenchymal stem cells. *Stem Cells*, *24*(7), 1750–1758.

Tan, M. L., Choong, P., & Dass, C. (2010). Recent developments in liposomes, microparticles and nanoparticles for protein and peptide drug delivery. *Peptides*, *31*(1), 184–193.

Tayalia, P., & Mooney, D. J. (2009). Controlled growth factor delivery for tissue engineering. *Advanced Materials*, *21*(32-33), 3269–3285.

Uebersax, L., Merkle, H. P., & Meinel, L. (2009). Biopolymer-based growth factor delivery for tissue repair: From natural concepts to engineered systems. *Tissue Engineering Part B: Reviews*, *15*(3), 263–289.

Wu, T., Zivanovic, S., Hayes, D. G., & Weiss, J. (2008). Efficient reduction of chitosan molecular weight by high-intensity ultrasound: Underlying mechanism and effect of process parameters. *Journal of Agricultural and Food Chemistry*, *56*(13), 5112–5119.